Electronic Supplementary Information (ESI)

Decorated high-dispersity $Fe(OH)_3$ nanoparticles on NiZn LDH nanosheets towards enhanced alkaline oxygen evolution reaction

Tianyi Yang,[a] Jianfeng Huang,[a] Zhaohui Liu*[a] and Cailing Chen*[b]

a. State Key Laboratory of Coal Mine Disaster Dynamics and Control, Institute of Advanced Interdisciplinary Studies, School of Chemistry and Chemical Engineering, Chongqing University, Chongqing 400044, China.

b. Advanced Membranes and Porous Materials (AMPM) Center, Physical Science and Engineering Division, King Abdullah University of Science and Technology (KAUST), Thuwal 23955, Saudi Arabia.

*Corresponding authors: zhaohui.liu@cqu.edu.cn (Dr. Z. Liu); cailing.chen@kaust.edu.sa (Dr. C. Chen);

Experimental section

Chemicals

Zinc acetate ($Zn(OAc)_2$), nickel acetate ($Ni(OAc)_2$), iron acetate ($Fe(OAc)_2$), 2-methylimidazole, potassium hydroxide were purchased from Aladdin industrial corporation(Shanghai, China). Ethanol, acetone, hydrochloric acid were obtained from Chron Chemicals (Chengdu, China). All the reagents are analytical grade and used without further treatment. Deionized (DI) water was employed as solvent.

Synthesis of NiZn nanosheet LDH array

A piece of NF (1 cm × 1 cm) was sonicated in 5% HCl solution, acetone, ethanol and water respectively for 15 min to obtain clean surface. In a typical synthetic procedure, 0.16 g $Zn(OAc)_2$, 0.09 g $Ni(OAc)_2$ were dissolved in 5 mL DI water and sonicated for 10 minutes to form homogeneous metal precursor solution. 0.20 g 2-methylimidazole were dissolved in 5 mL DI water and added into the metal precursor solution. Afterward, the mixed solution with the pre-treated NF were kept under room temperature overnight. The obtained NiZn precursors on NF was washed with ethanol and DI water, followed by dried at 60 °C.

Synthesis of NiZnFe nanosheet LDH array

The synthetic process was similar to NiZn nanosheet LDH array, except for a different weight of $Fe(OAc)_2$ (0.005 g, 0.010 g, 0.020 g, 0.040 g) were added into the metal precursor solution. According to metal weight percentage calculated from ICP results, the obtained samples were denoted as $NiZnFe_{2.6}$ LDH, $NiZnFe_{8.9}$ LDH, $NiZnFe_{12.9}$ LDH, $NiZnFe_{23.7}$ LDH, respectively.

Electrochemical measurements:

All electrochemical measurements were conducted in the three-electrode cell using Biologic SP300 potentiostat at room temperature. NF was used as the working electrode. The Hg/HgO and graphite rod were used as the reference and counter electrode, respectively. All potentials were converted into reversible hydrogen electrode (RHE), by following the formula E(RHE) = E(Hg/HgO) + 0.05916 × pH + 0.098. The electrolyte solutions were purged with high-purity O_2 for at least 30 min prior to each experiment. The working electrodes were firstly cycled between 0.2 V and 1.0 V vs. Hg/HgO at 50 mV s^{-1} in 1.0 M KOH for 30 cycles. LSV curves with 95%

iR-correction were acquired at a scan rate of 5 mV s^{-1}. Tafel plots of the overpotential vs. the log (current density) were recorded with linear portions at low overpotentials according to following equation $\eta = a + b\log j$, where η was the overpotential, b was the Tafel slope, j was the current density and a was the exchange current density.

EIS spectra were collected in the frequency range of 100 kHz-0.1 Hz with an overpotential of 20 mV. The electrochemical double layer capacitance (C_{dl}) was determined with typical cyclic voltammetry (CV) measurements at various scan rates (10, 20, 40, 60 and 100 mV s^{-1}) in 1.22~1.32 V vs. RHE. C_{dl} was calculated from the linear slope of $\Delta J/2$ versus scan rate, where ΔJ represents the difference in current density (ΔJ = positive current density –negative current density) at 1.27 V vs.RHE.

Characterization. (HR)TEM images and EDX elemental maps were acquired on Talos 200 S/TEM (Thermo Fisher Scientific) operated at 200 kV. XRD measurements were conducted on PANalytical X'Pert Powder using Cu Kα X-ray source. XPS data were collected on ESCALAB 250Xi XPS microprobe (Thermo Fisher Scientific) with a monochromatic Al Kα X-ray source under ultrahigh vacuum conditions. The data were analyzed by using the Avantage software. ICP-OES was performed on Spectro GREEN model to determine the metal concentration.

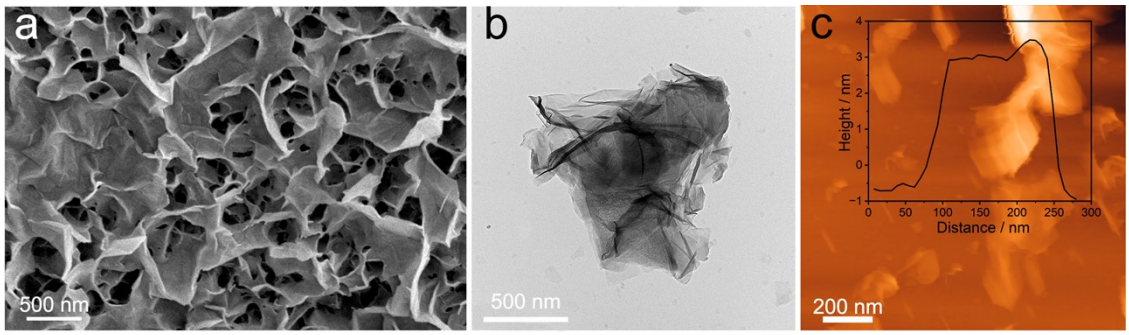

Fig. S1 SEM (a) TEM (b) AFM image and height profile (c) of NiZn LDH.

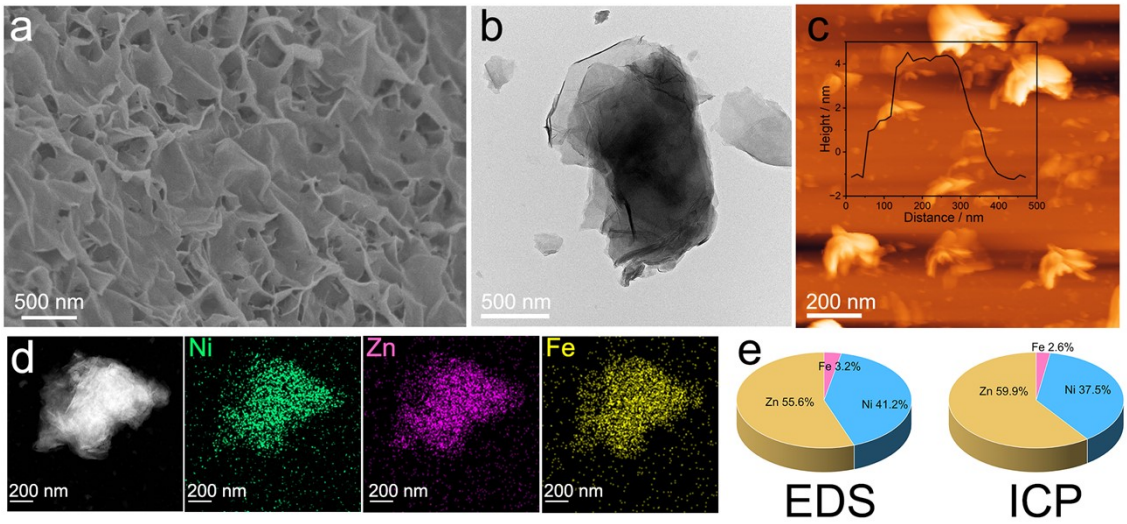

Fig. S2 SEM (a), TEM (b), AFM image height profile (c), HAADF-STEM and elemental mapping (d), EDS and ICP results (e) of $NiZnFe_{2.6}$ LDH.

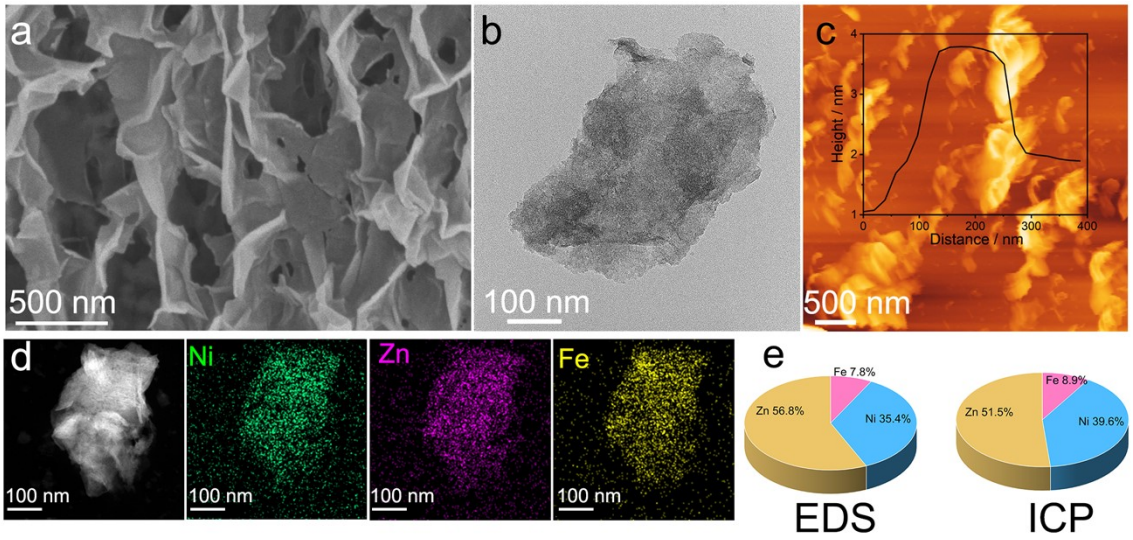

Fig. S3 SEM (a), TEM (b), AFM image height profile (c), HAADF-STEM and elemental mapping (d), EDS and ICP results (e) of $NiZnFe_{8.9}$ LDH

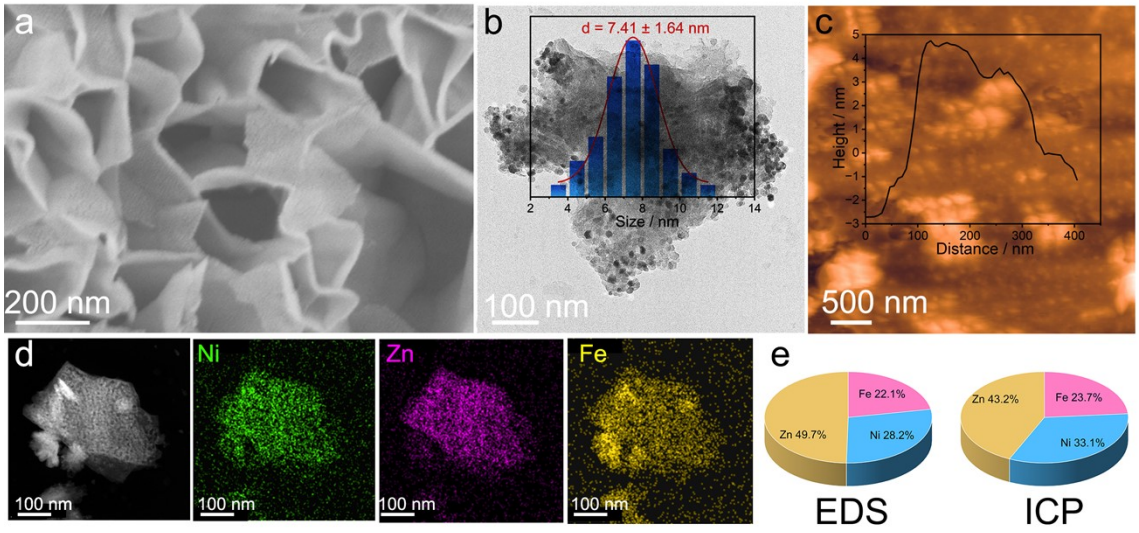

Fig. S4 SEM (a), TEM and $Fe(OH)_3$ size distribution (b), AFM image height profile (c), HAADF-STEM and elemental mapping (d), EDS and ICP results (e) of $NiZnFe_{23.7}$ LDH.

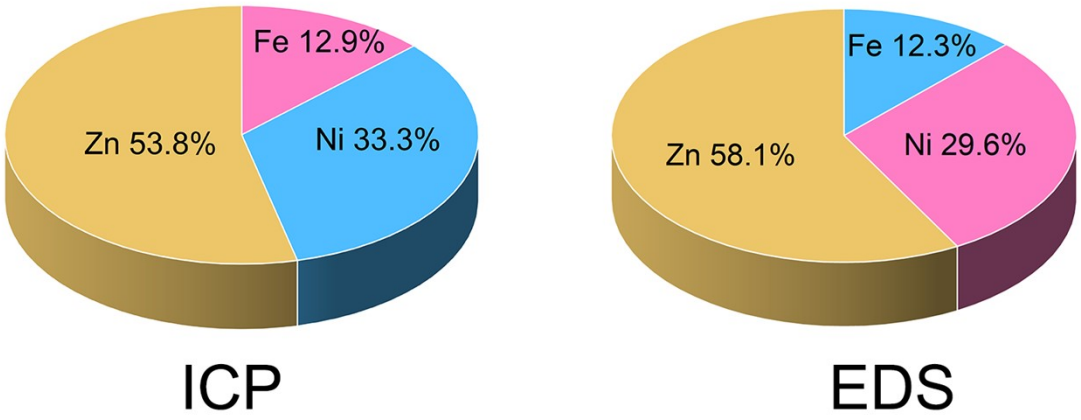

Fig. S5 ICP and EDS results of $NiZnFe_{12.9}$ LDH.

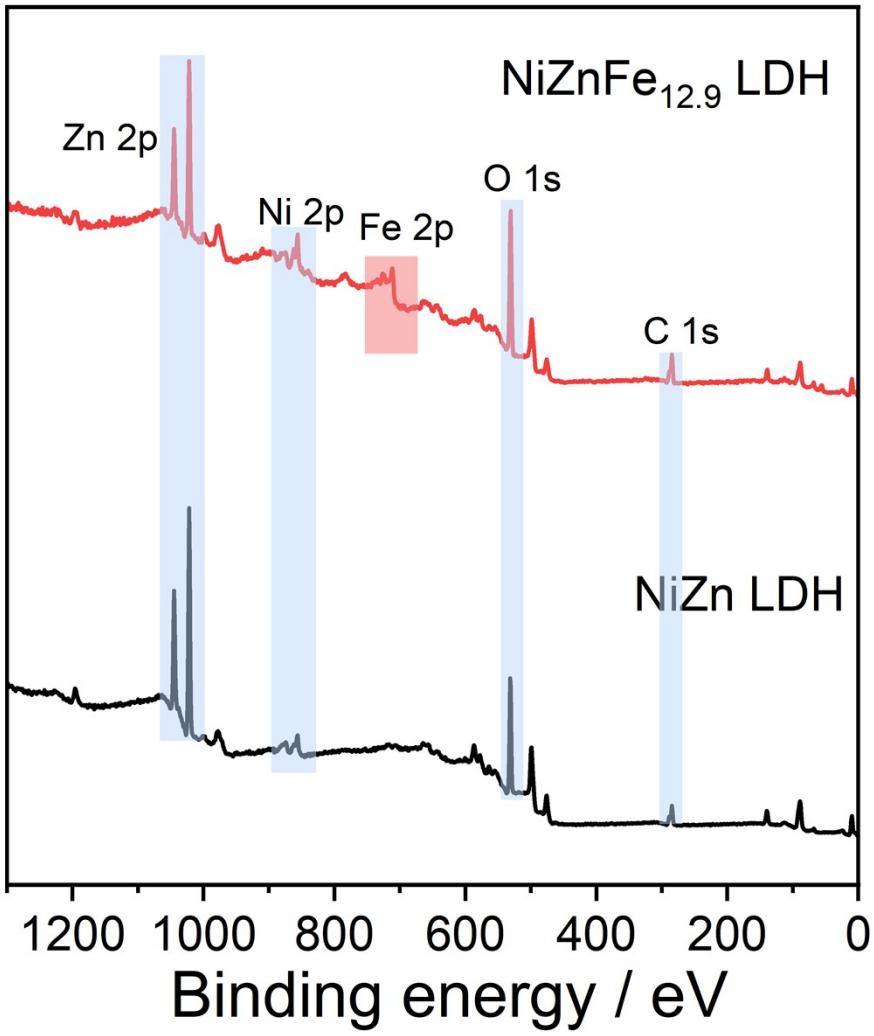

Fig. S6 XPS survey spectrum of NiZn LDH and $NiZnFe_{12.9}$ LDH.

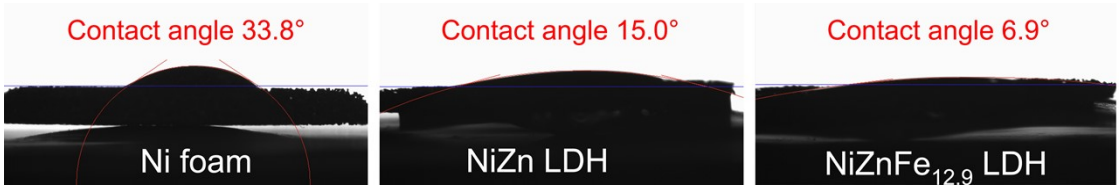

Fig. S7 The contact angle test of Ni foam, NiZn LDH and $NiZnFe_{12.9}$ LDH on Ni foam.

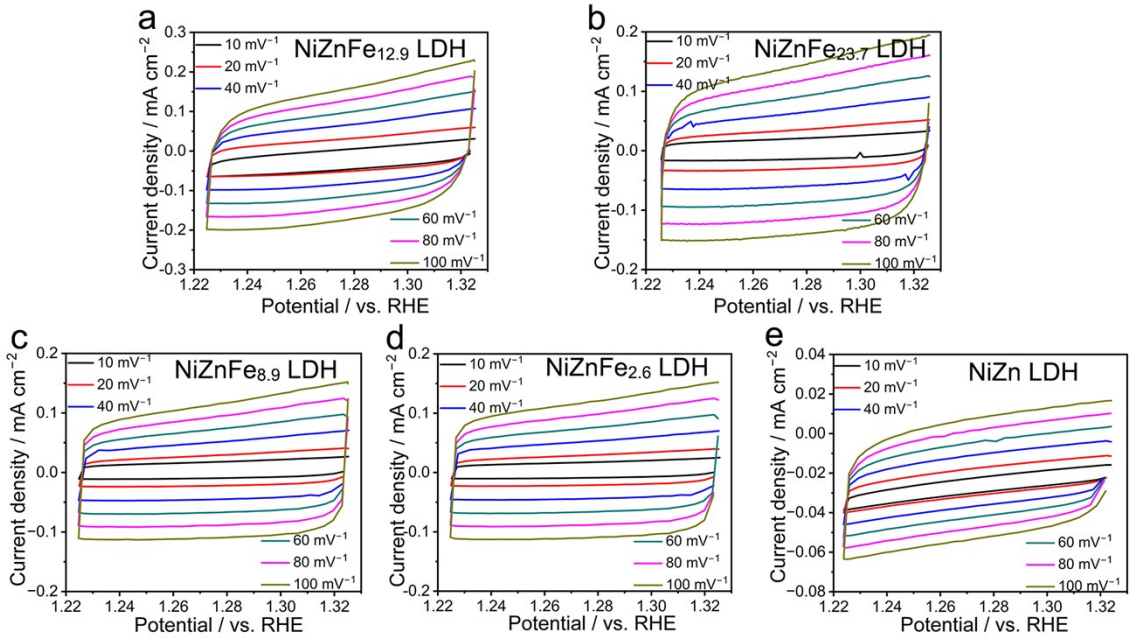

Fig. S8 CV curves of (a) $NiZnFe_{12.9}$ LDH, (b) $NiZnFe_{23.7}$ LDH, (c) $NiZnFe_{8.9}$ LDH, (d) $NiZnFe_{2.6}$ LDH and (e) NiZn LDH in the non-faradaic regions.

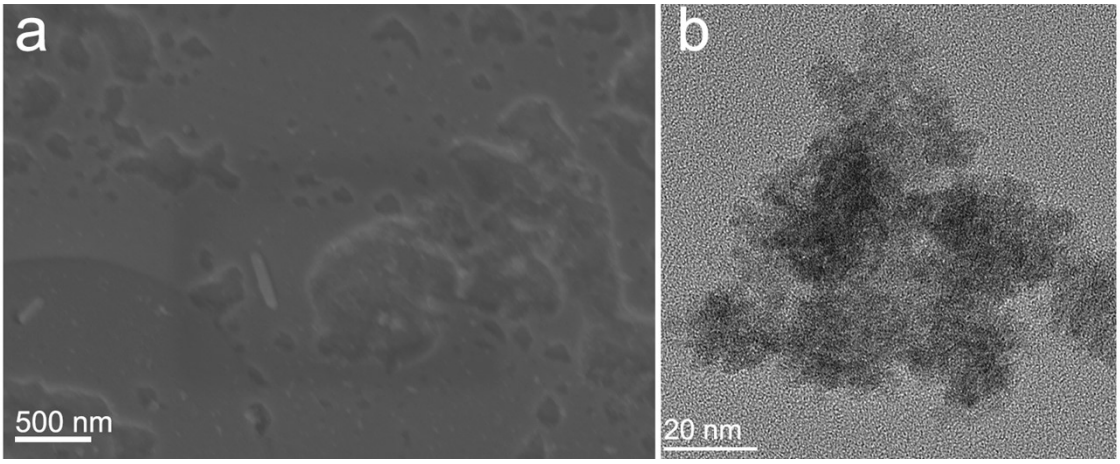

Fig. S9 The SEM (a) and TEM (b) images of $Fe(OH)_3$ nanoparticles.

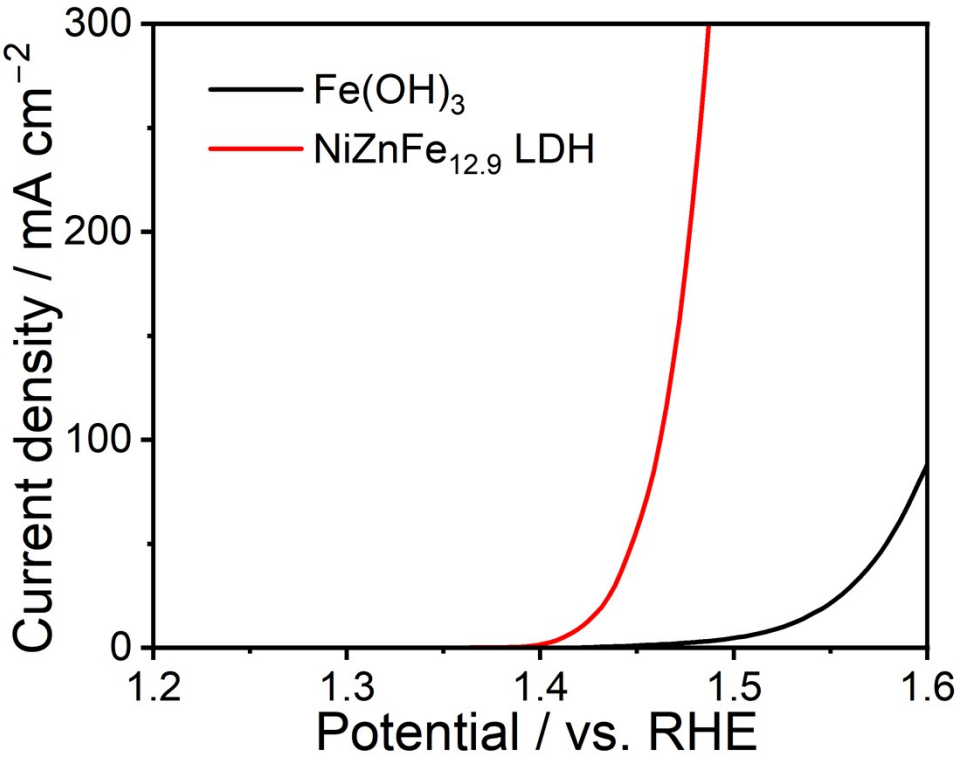

Fig. S10 LSV curves of $NiZnFe_{12.9}$ LDH and $Fe(OH)_3$ nanoparticles on Ni foam.

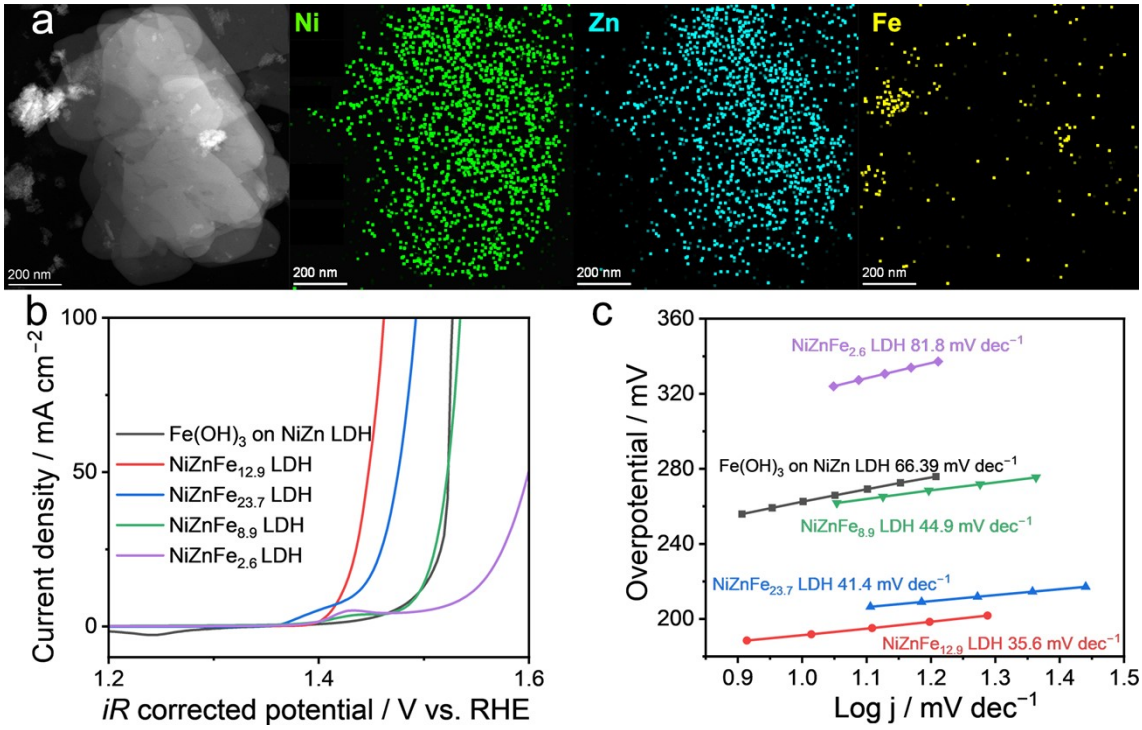

Fig. S11 (a) STEM and elemental mappings of $Fe(OH)_3$ on NiZn LDH nanosheets. (b) LSV curves and (c) Tafel slopes of different catalysts.

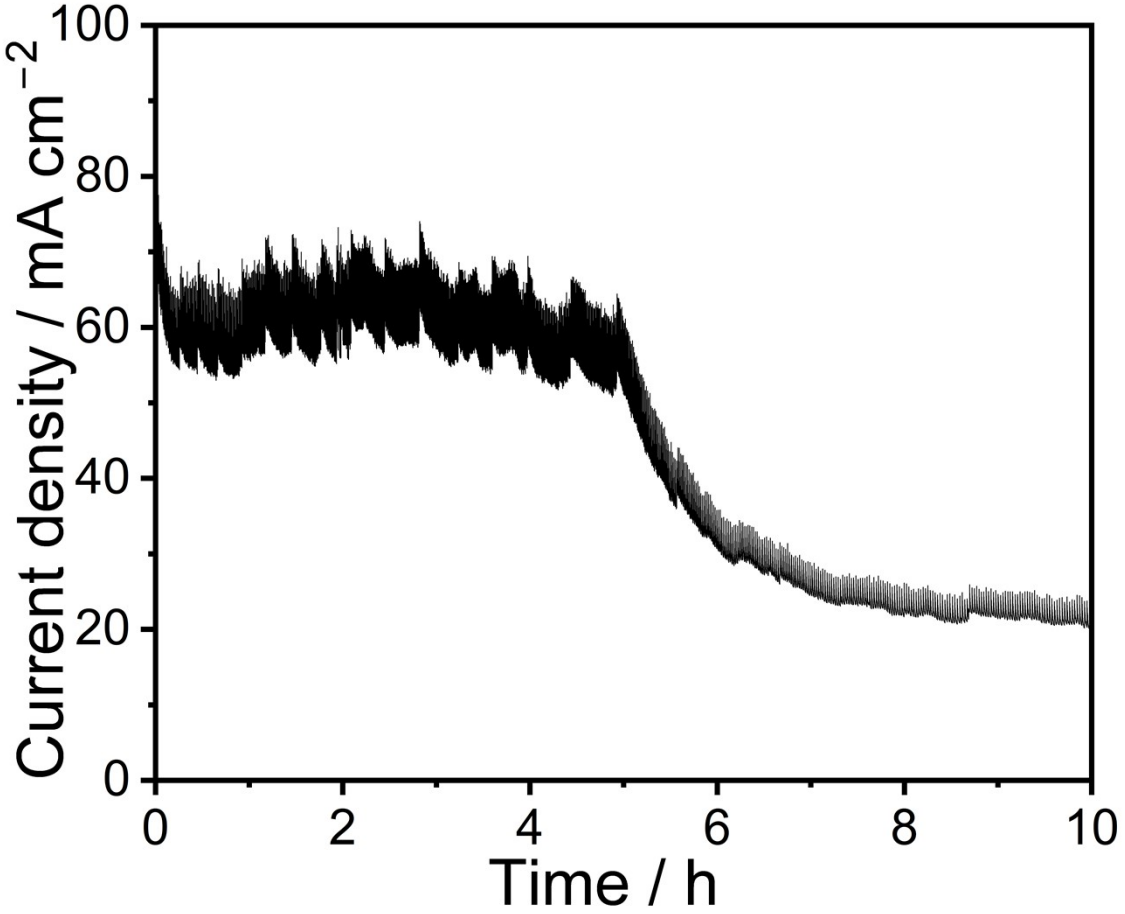

Fig. S12 The stability test of NiZn LDH.

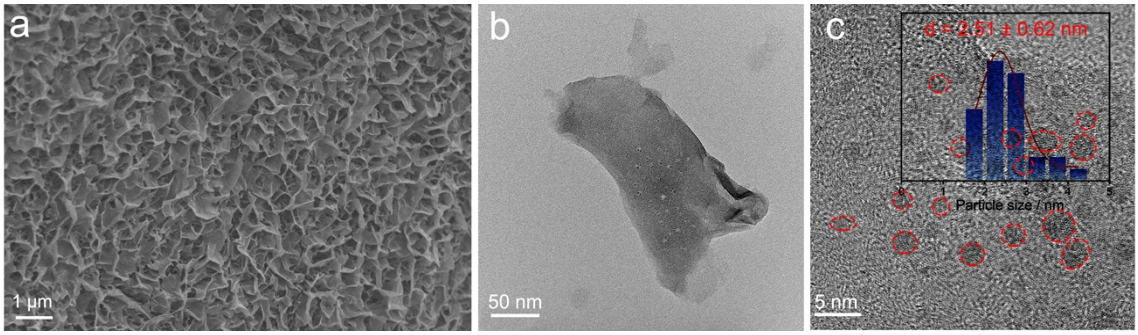

Fig. S13 SEM (a), TEM (b) and HRTEM (c) of $NiZnFe_{12.9}$ LDH after stability test.

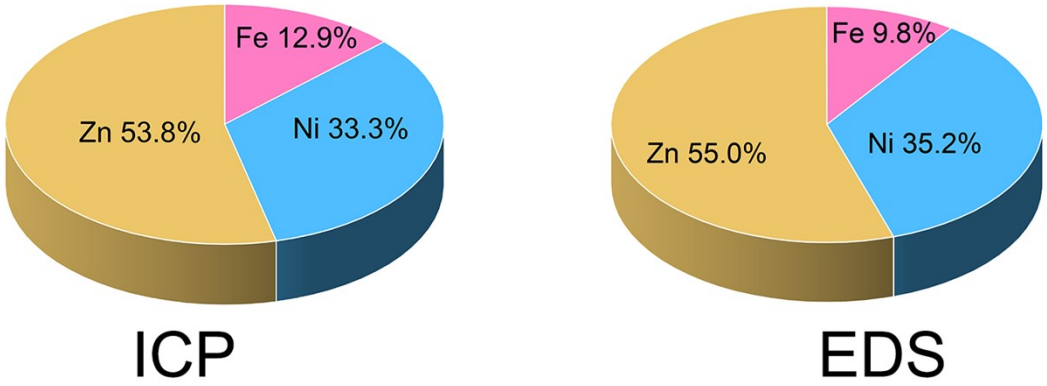

Fig. S14 ICP and EDS results of $NiZnFe_{12.9}$ LDH after stability test.

Table. S1 Comparison of Fe-containing catalysts for OER in 1 M KOH electrolyte

Catalysts	η_{10} (mV)	η_{100} (mV)	Tafel slope (dec mV^{-1})	Ref.
$NiZnFe_{12.9}$ LDH	**191**	**232**	**35.6**	**This work**
MIM@$Fe_{0.1}$-CoNi CH/NF	194	285	74.1	1
NiCoFe LDH/CNT/CC	200	239	32.4	2
Ni_3Fe-LDH	189	248	67.2	3
NiFe/B-TiO_x	227	268	37.5	4
R-NiFeOOH@SO_4		251	56	5
Pt-Co/Fe		285	48.76	6
Ultrathin NiFe LDH	210		31	7
NiFe–N–C	323		36	8
V_o-Fe–Co_3O_4	231	290	57.45	9
FeNiCo-MOF	239		42.4	10
Fe-Birnessite	240		33	11
Fe–MoO_2/NF		340	75	12
A-$Fe_2S_1N_5$/SNC	193		61	13
FeNiHOF	201	247	34.8	14
O_v-Fe MOF/IF	200		44	15
Fe-SACs|C–Ni@1	285		58	16
h-FeNi$(OH)_x$–NiS@$Ni(OH)_2$/NF	254.9		72.4	17
Ru_1/NiFe LDH	189	220	31	18
$Fe_{0.8}Ni_{0.15}S_{1.05}$	228		53	19
Fe–NH_2 MOF/NF	260	330	60.8	20

Table. S2 Comparison of solution resistance (R_s) and charge transfer resistance (R_{ct}) of different catalyst.

Catalysts	R_s (Ω)	R_{ct} (Ω)
$NiZnFe_{12.9}$ LDH	**1.364**	**2.038**
$NiZnFe_{23.7}$ LDH	1.765	2.056
$NiZnFe_{8.9}$ LDH	1.445	3.232
$NiZnFe_{2.6}$ LDH	1.595	3.301
NiZn LDH	2.176	5.648

Reference:

1. H. W. Tang, Z. Y. Sun, S. Y. Fan, S. W. Feng, L. Li, L. Fang and C. J. Wang, *Chem. Eng. J*, 2024, **491**, 152023.
2. X. Wang, Z. Qin, J. J. Qian, L. Y. Chen and K. Shen, *Appl.Catal.B-Environ.*, 2024, **359**, 124506.
3. J. Zhang, M. Li, Z. Q. Qiao, K. X. Huo, Y. Yang, D. Q. Ji, D. D. Yuan, L. Y. Lin, Z. D. Li and H. J. Wu, *J. Mater. Chem. A*, 2024, **12**, 2044.
4. T. X. Zhou, Y. F. Yang, Y. K. Jing, Y. L. Hu, F. Yang, W. Sun, and L. L. He, *Chem. Sci.*, 2023, **14**, 13453–13462.
5. X. Luo, H. Y. Zhao, X. Tan, S. Lin, K. S. Yu, X. Q. Mu, Z. H. Tao, P. X. Ji and S. C. Mu, *Nat. Commun.*, 2024, **15**, 8293.
6. Z. H. Zhang, Y. Zhang, A. Barras, A. Addad, P. Roussel, L. C. Tang, M. A. Amin, S. Szunerits and R. Boukherroub, ACS Appl. Energy Mater. 2022, 5, 15269–15281.
7. C. G. Kuai, Y. Zhang, D. Y. Wu, D. Sokaras, L. Q. Mu, S. Spence, D. Nordlund, F. Lin and X. W. Du, *ACS Cat*., 2019, **9** (7), 6027–6032.
8. H. B. Meng, B. Wu, D. T. Zhang, X. H. Zhu, S. Z. Luo, Y. You, K. Chen, J. C. Long, J. X. Zhu, L.P. Liu, S. B. Xi, T. Petit, D. S. Wang, X. M. Zhang, Z. C. J. Xu and L. Q. Mai, *Energy Environ. Sci.*, 2024, **17**, 704–716.
9. Q. Y. He, L. Han and Kai Tao, *Chem. Commun.*, 2024, **60**, 1116.
10. W. Q. Li, H. Zhang, K. Zhang, Z. Z. Cheng, H. P. Chen, G. Tan, X. Feng, L. Y. Wang and S. C. Mu, *Chem. Commun.*, 2023, **59**, 4750.
11. M. Ju, Z. W. Chen, H. Zhu, R. M. Cai, Z. D. Lin, Y. P. Chen, Y. J. Wang, J. L. Gao, X. Long and S. H. Yang, *J. Am. Chem. Soc.*, 2023, **145**, 20, 11215–11226.
12. J. P. Sun, S. Y. Qin, Z. Zhao, Z. S. Zhang and X. C. Meng, *Mater. Horiz.*, 2024, **11**, 1199–1211.
13. L. L. Zhang, N. Zhang, H. S. Shang, Z. Y. Sun, Z. H. Wei, J. T. Wang, Y. T. Lei, X. C. Wang, D. Wang, Y. F. Zhao, Z. T. Sun, F. Zhang, X. Xiang, B. Zhang and W. X Chen, *Nat. Commun.*, 2024, **15**, 9440.
14. Y. Z. Chen, Q. H. Li, Y. X. Lin, J. Liu, J. Pan, J. G. Hu and X. Y. Xu, *Nat Commun.*, 2024, **15**, 7278.
15. J. N. Song, S. Zhao, D. Liu, Y. X. Xiong, F. Hu, L. L. Li, L. Li, H. Pan and S. J. Peng, *Chem. Commun.*, 2022, **58**, 9662–9665.
16. A. Shankar, S. Marimuthu and G. Maduraiveeran, *J. Mater. Chem. A*, 2024, **12**, 121–127.
17. R. D. Shi, Y. T. Li, X. X. Xu, X. Wang and G. B. Zhou, *Adv. Funct. Mater.*, 2024, **34**, 2409849.
18. P. L. Zhai, M. Y. Xia, Y. Z. Wu, G. H. Zhang, J. F. Gao, B. Zhang, S. Y. Cao, Y. T. Zhang, Z. W. Li, Z. Z. Fan, C. Wang, X. M. Zhang, J. T. Miller, L. C. Sun and J. G. Hou, *Nat. Commun.*, 2021, **12**, 4587.
19. Z. X. Jing, Q. Y. Zhao, D. H. Zheng, L. Sun, J. H. Geng, Q. N. Zhou and J. J. Lin, *J. Mater. Chem. A*, 2020, **8**, 20323–20330.
20. N. K. Shrestha, S. A. Patil, S. Cho, Y. Jo and H. Kim, *J. Mater. Chem. A*, 2020, **8**, 24408–24418.